This is a Peer Reviewed Paper
FIG Working Week 2025

Forecasting Ionospheric Process Noise Using Long Short-Term Memory Network

Parvaneh Sadegh Nojehdeh and Kourosh Khoshelham, Australia

Key words: Ionospheric process noise, ionospheric time variation, prediction, LSTM, PPP-RTK

SUMMARY

Accurate ionospheric corrections generated by a precise point positioning real-time kinematic (PPP-RTK) provider can significantly improve the user integer ambiguity resolution (IAR) performance, enabling faster and more precise global navigation satellite systems (GNSS) positioning. However, to reduce the transmission rate of the corrections being sent to the user, ionospheric corrections are often delivered to users with latency. In such cases, the accuracy of user positioning depends on the dynamic model used to time-predict ionospheric corrections, as implemented in the Kalman filters of both the PPP-RTK provider and the user. This dynamic model inherently includes a degree of uncertainty, governed by the process noise variance of the corrections, which has a direct impact on the positioning accuracy. Therefore, specifying the process noise variance accurately is critical to minimizing the prediction error of ionospheric corrections. Although nominal values for the ionospheric process noise are commonly used, they can degrade the IAR performance and significantly reduce ambiguity-fixed positioning accuracy. Data-driven estimation of ionospheric process noise from GNSS observations significantly improve the IAR performance and ambiguity-fixed positioning accuracy. However, in scenarios where a user station has a historical record of ionospheric process noise, forecasting the process noise becomes a practical alternative. This study evaluates the forecasted ionospheric process noise and investigates its effect on IAR performance. We propose an approach based on a Long Short-Term Memory (LSTM) neural network to forecast ionospheric process noise, given an existing set of estimated values. LSTM models are particularly effective at capturing the ionosphere's dependencies on solar and geomagnetic activity, seasonal variations, and past ionospheric behavior. The model was validated using data from globally distributed GNSS stations, demonstrating low RMSE values (below 0.11 $mm/\sqrt{sec}$) across diverse geographic locations. The experiments confirmed that forecasted ionospheric process noise is a viable alternative to data-driven values, ensuring high IAR success rates. By providing reliable forecasts, this approach enables improved positioning accuracy and precision.

Forecasting Ionospheric Process Noise Using Long Short-Term Memory Network

Parvaneh Sadegh Nojehdeh and Kourosh Khoshelham, Australia

1. Introduction

Precise point positioning in real-time applications, such as precise point positioning real-time kinematic (PPP-RTK), relies on accurate ionospheric delay corrections. When a PPP-RTK provider supplies precise ionospheric corrections, it significantly enhances user integer ambiguity resolution (IAR) performance, enabling faster and precise global navigation satellite systems (GNSS) positioning (Collins et al. 2012; Odijk et al. 2016; Zha et al. 2021). To reduce the transmission rate, this correction may be provided to the PPP-RTK user with a time delay or latency (Wübbena et al. 2005). In such cases, the quality of the user's position depends on the accuracy of the dynamic model used for ionospheric corrections, which is employed by the Kalman filter of the PPP-RTK provider to time-predict the corrections (Psychas et al. 2022). A constant-state dynamic model may effectively capture the ionosphere dynamic behavior, provided that the delay between the correction generation time by the provider and the time that user applies the corrections to their data is sufficiently short, e.g., less than 1 minute (Khodabandeh 2021; Sadegh Nojehdeh et al. 2024b).

The dynamic model inherently involves a degree of uncertainty, determined by the process noise variance of this correction, which directly impacts positioning quality. Therefore, in addition to accurately specifying the dynamic model of ionosphere correction, accurately defining the process noise variance of the ionosphere is essential to minimize large prediction errors, as inaccuracies can lead to significant losses in the precision of parameter solutions. Despite the importance of accurately specifying this parameter, many previous studies have relied on using nominal values, e.g., $1\ mm/\sqrt{sec}$. Psychas et al. (2022) highlighted the importance of correctly specifying the process noise for PPP-RTK corrections. Following that study, Sadegh Nojehdeh et al. (2024a, b) explored the limitations of using nominal ionospheric process noise values, demonstrating that such an approach can degrade IAR performance and significantly impact ambiguity-fixed positioning accuracy. They emphasized the critical importance of incorporating spatiotemporal-dependent ionospheric process noise in the parameter estimation process for both PPP-RTK providers and users.

Furthermore, they introduced a straightforward algorithm to estimate ionospheric process noise. By analyzing up to 11 years of data from globally distributed GNSS stations, they demonstrated how the dynamic nature of ionospheric process noise is influenced by solar and geomagnetic activity, as well as seasonal variations. They also showed that nearby stations, within a range of up to 300 km, produce similar ionospheric process noise estimates. Consequently, if a provider accurately determines the ionospheric process noise, nearby users can benefit from using the same value.

Data-driven estimation of ionospheric process noise from GNSS observations significantly improves IAR performance and ambiguity-fixed positioning accuracy. However, in scenarios where a user station has access to a historical record of ionospheric process noise, forecasting the process noise becomes a practical alternative. By using historical data and models that

account for the ionosphere's spatiotemporal variability, users can achieve accurate positioning results even in the absence of data-driven ionospheric process noise estimation. This predictive approach offers ionospheric process noise values that improve positioning accuracy and enhance the reliability PPP-RTK method.

In this paper, we propose an approach based on Long Short-Term Memory (LSTM) neural network to forecast ionospheric process noise. LSTM models are particularly suited for this task since the ionosphere's temporal variability is influenced by multiple factors, including solar and geomagnetic activity, as well as seasonal variations (Hernández-Pajares et al. 2011). These factors create time-dependent patterns in ionospheric process noise, making LSTM an effective method for modeling and forecasting this variability (Ruwali et al. 2020; Wen et al. 2021). By capturing these dynamic dependencies, the LSTM model provides reliable forecasts, enhancing positioning accuracy even in the absence of real-time corrections.

The structure of this paper is organized as follows: We begin by presenting the LSTM method. Next, we provide results and discussion, detailing the dataset used, the proposed LSTM network, an ablation study to determine feature importance, and validating the effectiveness of the proposed LSTM model for other GNSS stations. We also demonstrate the effect of the forecasted ionospheric process noise on the IAR success rate. Finally, we conclude the paper with a summary of key findings.

2. Ionospheric process noise forecasting method and experiments

Given a time series of ionospheric process noise over the past n days, along with associated feature time series, the objective is to forecast the ionospheric process noise for the next m days. In this study, we utilized the LSTM's capability to model temporal dependencies for forecasting ionospheric process noise. This section begins with an overview of the LSTM network, followed by a description of our experimental setup. We detail the preparation of the features and target time series for training the network. Additionally, we describe the proposed LSTM network architecture determined through experimentation, including training processes, the optimization metric, and relevant configurations. Finally, we explain the forecasting process and the metric used to evaluate forecasting performance.

2.1 LSTM network

Long Short-Term Memory (LSTM) networks are a type of recurrent neural network (RNN) specifically designed to learn effectively from data sequences with long-term dependencies (Hochreiter and Schmidhuber, 1997). Unlike traditional RNNs, which often struggle with vanishing or exploding gradients over long sequences, LSTMs incorporate specialized gating mechanisms, namely, input, forget, and output gates, that enable the network to selectively remember or discard information. This capability makes LSTMs particularly well-suited for time-series forecasting, where understanding past states is essential for improving predictions of future values.

Figure 1 shows the overall architecture of the LSTM network used in this study. The network includes a sequence input layer, a single LSTM layer to capture temporal dependencies across a time window, a fully connected layer to process learned features, and a regression output layer to generate the forecasted ionospheric process noise. The LSTM layer consists of multiple sequentially connected LSTM cells, where each cell processes the input data step by step and

passes relevant information to the next cell, effectively capturing patterns in the temporal sequence.

Figure 2 focuses on the internal structure of a single LSTM cell, highlighting the interactions between the gates and the cell state. Each LSTM cell consists of three primary gates, including forget gate (f_t), input gate (i_t), and output gate (o_t), as well as a cell state (C_t) and hidden state (h_t). The forget gate, implemented using a sigmoid function (σ), determines how much information from the previous cell state (C_{t-1}) should be retained, allowing the model to "forget" irrelevant data. The input gate, also managed by a sigmoid function, regulates which new information should be added to the cell state. It works in conjunction with a *tanh* activation function to create an update, which is integrated into the cell state. The output gate, controlled by another sigmoid function, determines what information from the current cell state should be passed to the next hidden state (h_t), for the subsequent timesteps. The cell state (C_t) serves as a memory that flows through the cell, retaining crucial information across timesteps (Goodfellow et al. 2016).

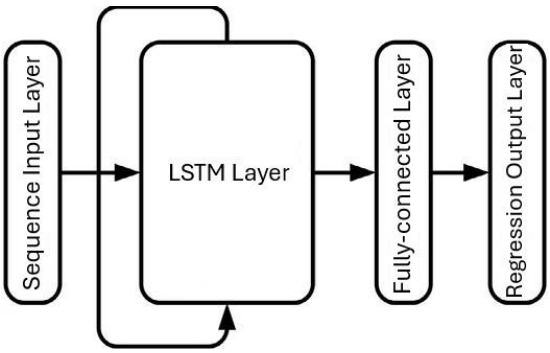

Fig 1. Architecture of an LSTM network for regression tasks, used to forecast ionospheric process noise in this study. The network consists of a sequence input layer, a single LSTM layer to capture temporal dependencies, a fully connected layer, and a regression output layer to generate forecasts.

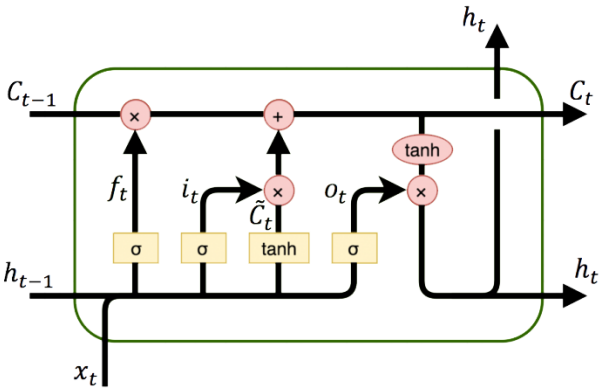

Fig 2. LSTM cell structure with memory and gating mechanisms for capturing long-term dependencies. The cell includes input, forget, and output gates, along with the cell state and hidden state, illustrating how information flows and is regulated across timesteps (Sun et al. 2017).

These gating mechanisms enable LSTMs to selectively remember or forget information, making them highly effective for tasks like time-series forecasting. By addressing the limitations of traditional RNNs, such as vanishing and exploding gradients, LSTMs provide a robust solution for capturing long-term dependencies in sequential data (Hochreiter and Schmidhuber, 1997; Bengio et al., 1994).

This study uses these capabilities of LSTMs to model and forecast the temporal dynamics of ionospheric process noise, accounting for its relationships with external factors such as solar activity, geomagnetic activity, and seasonal variation. In the following subsections, the inputs and the output of this study, as well as the design of the proposed LSTM network, are described.

2.2 Inputs and output description

For the output (target) time series, we used data-driven ionospheric process noise from three globally distributed GNSS stations: SGOC, CUT0, and PALM, located in low-, mid-, and high-latitude regions, respectively (Sadegh Nojehdeh et al. 2024). For CUT0, 11 years of ionospheric process noise data (2013–2023) were available, while for SGOC and PALM, data spanning 5 years (2019–2023) were used, covering both solar minimum and solar maximum periods. These stations were selected to ensure geographic diversity, as shown in Table 1, which provides details on station locations.

Given the correlation between ionospheric process noise and both solar flux index F10.7 and Kp index, these parameters were included as two of the input (feature) time series. To account for seasonal patterns, sine and cosine functions with a one-year period ($T = 365$) were also incorporated to capture periodic variations. Figure 3 demonstrates the time series of the target and external features, with the top three panels showing daily ionospheric process noise for the three stations, and the remaining panels representing the feature time series.

The LSTM network was trained separately for each station, with CUT0 serving as the main dataset for network design and ablation study. For SGOC and PALM, the proposed LSTM network was cross-checked to ensure consistency. Since the target time series contains occasional missing days, only days with available target data were used for the input time series. For the solar flux index and Kp index time series, data corresponding to the missing days were excluded. Similarly, for the sine and cosine components, $\sin(2\pi t/T)$ and $\cos(2\pi t/T)$, t was filled only for the available days, omitting entries for the missing days. These features were extracted exclusively for these aligned days to maintain consistency across all input features and the target time series.

The temporal sequence of the target variable (autoregressive), combined with real-time external features, forms the feature matrix for each sample. This setup allows the model to capture temporal dependencies within the target variable and learn from its own historical patterns, trends, and behaviors while incorporating influential external factors. The input features consisted of the previous ionospheric process noise, the current solar flux index, the Kp index, and sine and cosine functions, all of which were fed into the LSTM network.

For a time window W, each sample of ionospheric process noise at time t, σ_t, includes a sequence of past target values $[\sigma_{t-W}, \sigma_{t-W+1}, \dots, \sigma_{t-1}]$. Alongside these past values, external features measured at the current time step t, are included as features; solar flux index (sf_t), Kp

index (kp_t), and seasonal variations represented as sine (s_t) and cosine (c_t) components. Thus, the feature matrix for each sample is structured as follows

Table 1. Geographic locations of the GNSS stations analyzed in this study. The station SGOC is located in the Northern Hemisphere, while CUT0 and PALM are in the Southern Hemisphere.

Stations	Country	Lat (◦)	Lon (◦)
SGOC	Sri Lanka	7	80
CUT0	Australia	− 32	116
PALM	Antarctica	− 65	− 64

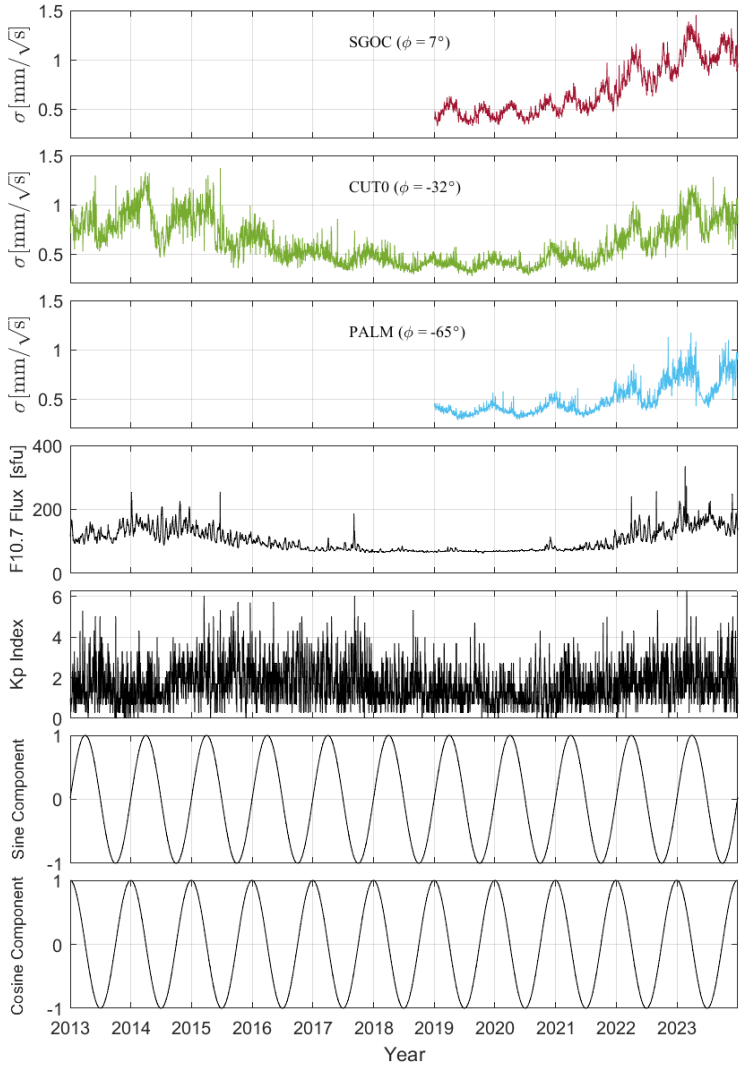

Fig 3. Time series data utilized in this study. The top three panels show the target time series (ionospheric process noise) for stations SGOC, CUT0, and PALM, respectively. The fourth and fifth panels present the daily solar flux index F10.7 and the Kp index, while the bottom two panels show the sine and cosine components used to model seasonal variations.

$$X = \begin{bmatrix} \sigma_{t-W} & sf_{t-W+1} & kp_{t-W+1} & s_{t-W+1} & c_{t-W+1} \\ \sigma_{t-W+1} & sf_{t-W+2} & kp_{t-W+2} & s_{t-W+2} & c_{t-W+2} \\ \vdots & \vdots & \vdots & \vdots & \vdots \\ \sigma_{t-2} & sf_{t-1} & kp_{t-1} & s_{t-1} & c_{t-1} \\ \sigma_{t-1} & sf_t & kp_t & s_t & c_t \end{bmatrix} \quad (1)$$

where X is a $W \times 5$ matrix representing the five features across the time window. The corresponding target, $y = \sigma_t$, is the ionospheric process noise at time t.

To prepare the data, all features and targets were normalized to ensure consistent scaling, facilitating efficient learning within the LSTM network. The dataset was divided into training, validation, and testing subsets to support model development and evaluation. This comprehensive preparation of the target and feature datasets lays the foundation for designing and testing the proposed LSTM network, as detailed in the following subsection.

2.3 Proposed LSTM network

The proposed LSTM network architecture consists of a single LSTM layer with 50 hidden units, followed by a fully connected layer. Initial trials with a more complex architecture, incorporating two LSTM layers separated by a dropout layer, demonstrated decreased training performance, increased loss function value. This finding indicated that the simpler single-layer architecture was more effective for the task. Additionally, increasing the number of hidden units beyond 50 reduced the RMSE by less than 1%, which we consider negligible based on the benchmark for the IAR success rate (99.9%) computed using forecasted ionospheric process noise. Consequently, the architecture with 50 hidden units was selected as it provided a balance between model complexity and forecasting accuracy.

The input sequence was structured using a sliding window approach with a window size of 60 time steps, allowing the network to learn from the previous 60 days of data to predict the subsequent day's ionospheric process noise. During the testing phase, the model employed recursive forecasting, where each forecasted target value along with other features were fed back into the model as an input for subsequent predictions, enabling continuous forecasting over extended periods.

The network was trained using the Adam optimizer with an initial learning rate of 0.001. The Adam optimizer dynamically adapts the learning rate for each parameter, enhancing convergence and improving training stability. A gradient threshold of 1 was applied to prevent gradient explosions during training. The training process was limited to a maximum of 50 epochs, with early stopping criteria to prevent overfitting if validation loss stopped improving. The LSTM network was implemented in MATLAB, and the training options were carefully configured to minimize overfitting and achieve optimal convergence. Table 2 summarizes the architecture parameters and values used in the experiments.

The loss function used during training is mean squared error (MSE)

$$MSE = \frac{1}{n}\sum_{i=1}^{n}(y_i - \hat{y}_i)^2 \quad (2)$$

where n is the total number of time steps in the training and validation datasets, y_i represents the observed value of the target variable (ionospheric process noise) at the i-th time step, and $\hat{y}_i$ represents the predicted value generated by the LSTM model for the same time step. The MSE measures the average squared difference between the observed values and the predicted values, serving as a quantitative indicator of the model's prediction accuracy.

Table 2: LSTM network architecture parameters and values.

Parameter	Value
Input Size	5
Output Size	1
Sequence length	60 days (sliding window)
Hidden units	50
Optimizer	Adam
Gradient Threshold	1
Initial Learning Rate	0.001
Max epochs	50
Loss function	MSE

2.4 Forecasting with the proposed LSTM network

The trained LSTM network is used to forecast ionospheric process noise over future time steps. In this study, the model is provided with a sequence of past target values and present external feature values to predict the ionospheric process noise for the next time step. The forecasted value is then recursively fed back into the model, along with external features, for subsequent time steps, enabling multi-step forecasting over an extended period. This approach allows the model to adapt to time-varying patterns in ionospheric process noise while capturing relationships between input features and the target variable.

The root mean square error (RMSE) was used to assess forecasting performance during evaluation. The mathematical formulation for RMSE is as follows

$$RMSE = \sqrt{\frac{1}{m}\sum_{i=n+1}^{n+m}(y_i - \hat{y}_i)^2} \qquad (3)$$

where m is the number of time steps in the test dataset, y_i represents the observed value of the ionospheric process noise at the i-th time step, and $\hat{y}_i$ denotes the corresponding forecasted value generated by the LSTM model. RMSE is useful for assessing forecasting performance, as it penalizes larger errors more heavily than smaller ones, emphasizing the importance of accurate predictions.

3. Results and discussion

We applied the LSTM method to the target and feature time series to train the network and forecast ionospheric process noise for future time steps. First, we trained the proposed LSTM network using data from the CUT0 station and conducted an ablation study to evaluate the importance of different features. Next, we applied the designed LSTM network to features and ionospheric process noise data from other globally distributed GNSS stations. Finally, we assessed the impact of the forecasted ionospheric process noise on the IAR success rate.

3.1 Forecasting ionospheric process noise for CUT0 station

We used the LSTM network architecture to train the model in three separate attempts for CUT0. In the first attempt, data from 2013 to 2020 was used for training and validation, with 2021 designated for testing. In the second attempt, data from 2013 to 2021 was used for training and validation, and 2022 was used for testing. Finally, in the third attempt, data from 2013 to 2022

was used for training and validation, with 2023 reserved for testing. For all attempts, 5% of the data was allocated for validation, while the remaining data was used to train the network.
Figure 4 shows the loss and validation curves for the three attempts, respectively. The loss curve is shown for every iteration, while the validation curve is shown at intervals of 50 iterations, with both curves demonstrating strong convergence. Figure 5 demonstrates the corresponding forecasted time series for each testing year, 2021, 2022, and 2023. The RMSE values for the predictions were calculated as 0.06, 0.08, and 0.11 $mm/\sqrt{sec}$ for 2021, 2022, and 2023, respectively. Based on these results, there is a potential indication that the model may perform better during periods of low solar activity.

3.2 Ablation study

While the proposed LSTM network demonstrated strong performance in forecasting ionospheric process noise for the CUT0 station using all input features, understanding the contribution of individual features to the model's forecasting performance is essential. To address this, we conducted an ablation study to evaluate the contribution of different features to the model's predictive performance.
Initially, we used only past target values as features and progressively added the external features one by one; the solar flux index, Kp index, and seasonal variation components (sine and cosine functions). We also tested the case where only external features (excluding past target values) were used. All these combinations were compared with the baseline case where all features, including past target values and external features, were included. For each combination, we used data from the CUT0 station spanning 2013 to 2023.
In each experiment, the model was trained and validated using four years of data and tested on one year. Afterward, we shifted the window forward by one month and repeated the process, again using four years of data for training and validation (with 5% allocated for validation) and one year for testing. This sliding window approach was repeated until the entire dataset was processed. For each feature combination, we computed the RMSE values, which were used to generate histograms of the RMSE distributions.
Figure 6 shows the RMSE histograms for different feature combinations. The results indicate that incorporating past target values (σ) alongside to external features (sf, kp, sv) improves model performance (left-top panel). However, for long-term predictions (1 year), using only past target values does not yield optimal performance (right-top panel). Based on the other combinations, the solar flux index and seasonal variation components emerged as the most important features, while the Kp index had less impact. Notably, none of these external features alone combined with past target values provided better performance.
The relatively low correlation between ionospheric process noise and the Kp index at CUT0 explains why the Kp index did not significantly improve prediction performance for this station. However, this observation does not apply to high-latitude stations, where ionospheric process noise is strongly correlated with the Kp index. Similarly, the solar flux index is expected to have a more pronounced impact for stations located in equatorial regions (Sadegh Nojehdeh et al., 2024).

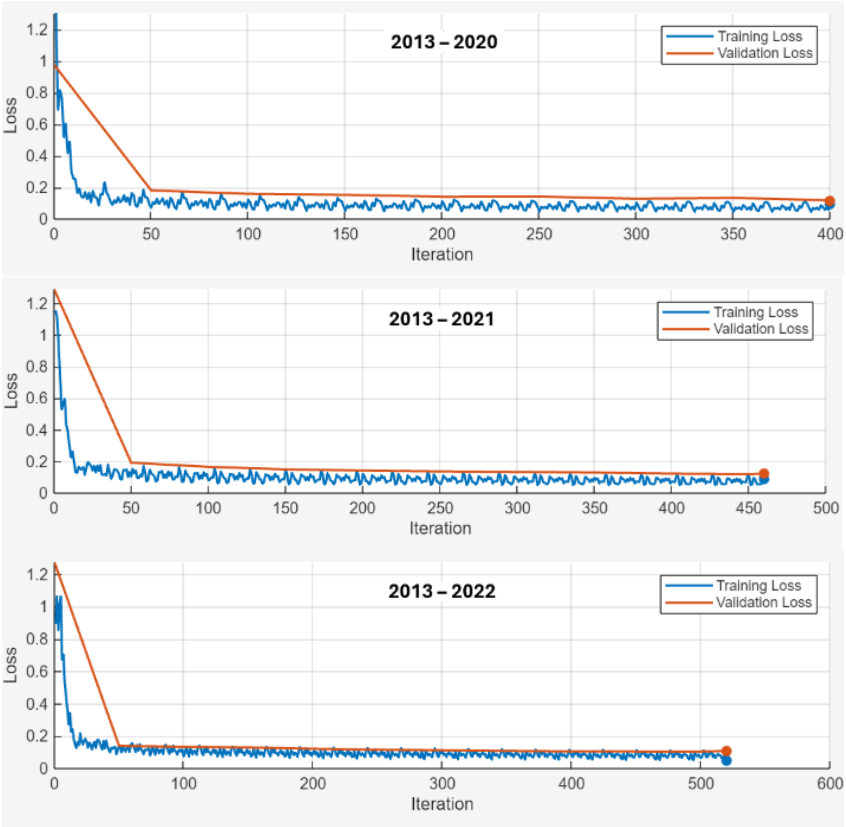

Fig 4. Loss and validation curves during training for the periods 2013–2020, 2013–2021, and 2013–2022. The loss curve is plotted for every iteration, while the validation curve is shown every 50 iterations.

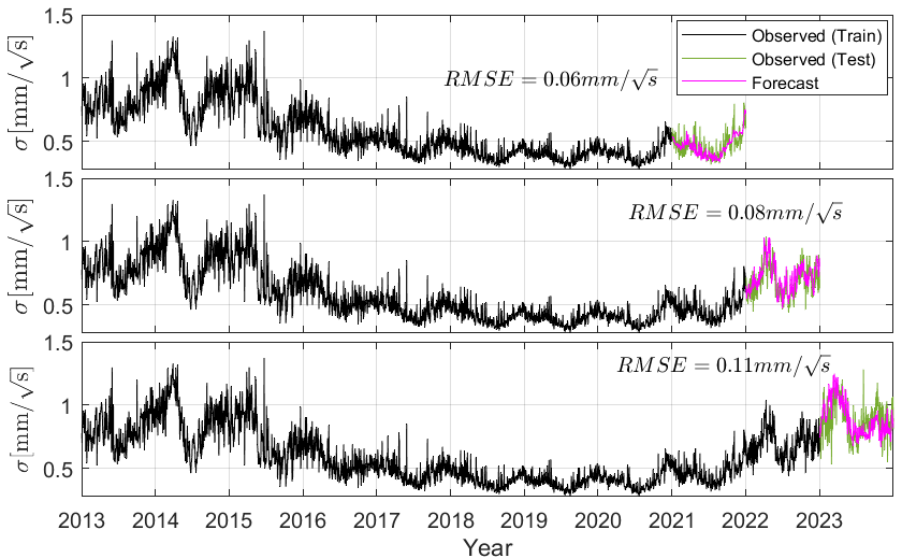

Fig 5. Forecasted ionospheric process noise time series for testing years 2021, 2022, and 2023. Forecasted time series reflect the model's performance, with RMSE values of 0.06, 0.08, and 0.11 $mm/\sqrt{sec}$ for the respective testing years.

We repeated this analysis for short-term predictions, using 1-month testing periods instead of 1-year periods. The results were consistent with the first experiment, as shown in Figure 7, which compares the histograms for two scenarios, when only past target values were used as features σ, and when all features were included (σ, sf, kp, sv). For short-term predictions, external features such as the solar flux index and seasonal components were not necessary, as past target values alone provided predictions relatively comparable to those achieved with all features. However, this may not hold for stations located in equatorial or high-latitude regions, where ionospheric process noise is strongly correlated with the solar flux index and Kp index, respectively.

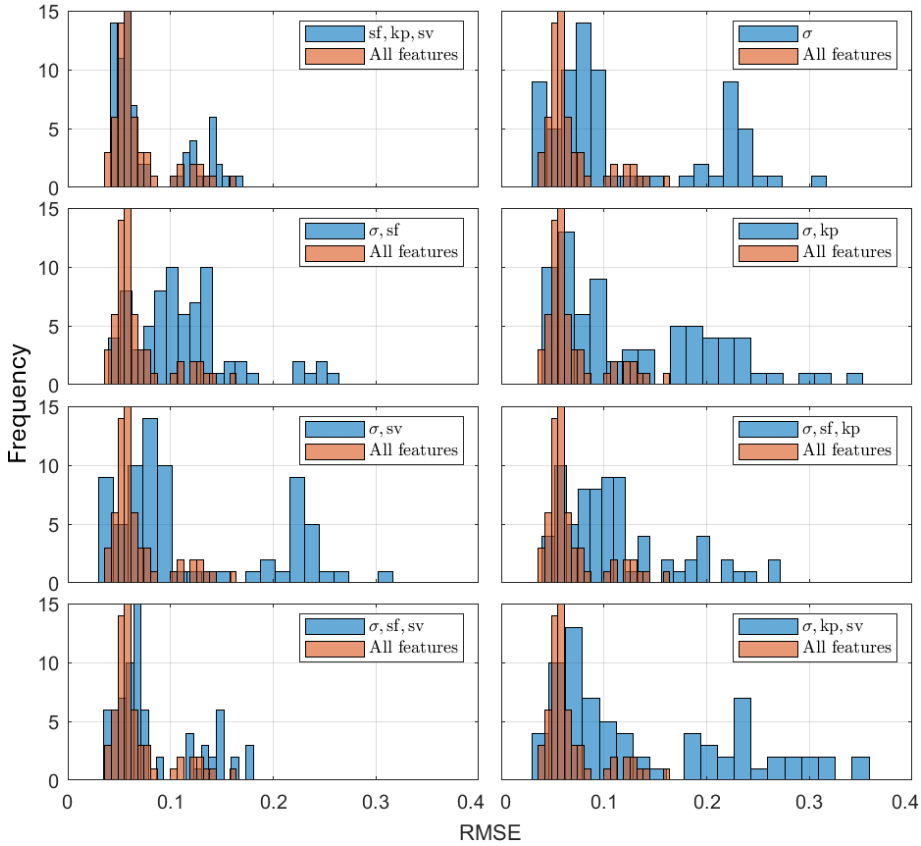

Fig 6. Histograms of RMSE values for different feature combinations in the ablation study using data from the CUT0 station (2013–2023), with a 1-year test data window. The histogram contains 20 bins.

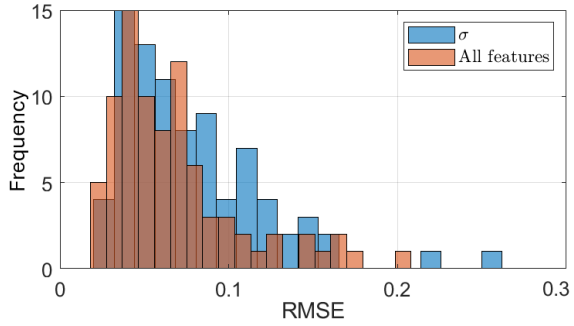

Fig 7. Histograms of RMSE values for two feature combinations in the ablation study using data from the CUT0 station (2013–2023), with a 1-month test data window. The histogram contains 20 bins.

3.3 Extending the analysis to globally distributed GNSS stations

To assess the generalizability of the proposed LSTM network, we extended the analysis to globally distributed GNSS stations. The LSTM network was further trained and tested on data from two additional GNSS stations, SGOC, located in the low-latitude (equatorial) region, and PALM, located in the high-latitude region. For both stations, four and a half years of data (from 2019 to Jun 2023) were used for training and validation (5% allocated for validation), with six months (July to December 2023) reserved for testing. All features were used to forecast the ionospheric process noise for these six months. Figure 8 shows the forecasted time series for SGOC and PALM. The RMSE values for the predictions were 0.09 and 0.1 $mm/\sqrt{sec}$, respectively.

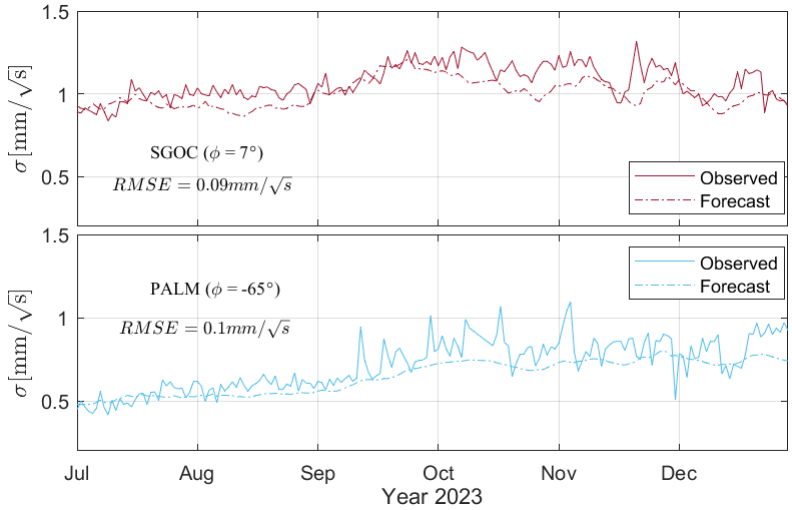

Fig 8. Forecasted time series of ionospheric process noise for the SGOC and PALM stations, located in equatorial and high-latitude regions, respectively. The LSTM network was trained using four and a half years of data, with six months reserved for testing. RMSE values for the predictions were 0.09 $mm/\sqrt{sec}$ for SGOC and 0.1 $mm/\sqrt{sec}$ for PALM.

3.4 Impact of forecasted ionospheric process noise on IAR success rate

Sadegh Nojehdeh et al. (2024) demonstrated that user IAR performance can significantly deteriorate if the nominal values of ionospheric process noise differ substantially from their true values. To address this, they proposed directly determining ionospheric process noise using GNSS data. In this study, we provide a forecast for the ionospheric process noise, which serves as a nominal value. Therefore, it is crucial to evaluate the IAR performance when the forecasted ionospheric process noise is used.

To this end, we selected one month from a low solar activity period, January 2021, from the CUT0 station. This month was chosen because the difference between the data-driven and commonly used nominal ionospheric process noise value ($1\,mm/\sqrt{sec}$) is particularly pronounced during periods of low solar activity. We computed the IAR success rate under three

scenarios: (1) when the observed (data-driven) ionospheric process noise was applied, (2) when the forecasted value was used, and (3) when the commonly used nominal value of 1 $mm/\sqrt{sec}$ was provided to the user receiver. For all scenarios, a latency of 8 seconds in providing ionospheric corrections was assumed. GPS and Galileo phase and code measurements were used for a single epoch at 02:00 GPS Time. Detailed information regarding the GNSS data, IAR method, and parameter configurations for the stochastic and dynamic models is presented in Table 3.

Figure 9 presents the computed IAR success rates for the three scenarios. When the forecasted ionospheric process noise was used, the success rate most of the days exceeded 99.9%, a level typically required for surveying applications. However, the commonly used nominal value of 1 $mm/\sqrt{sec}$ resulted in success rates below 98%.

These results emphasize the critical importance of accurately specifying ionospheric process noise. Forecasted ionospheric process noise ensures high IAR success rates, particularly during periods of low solar activity when nominal values deviate significantly from true values. This approach is especially advantageous for users in environments with limited access to GNSS stations, enabling reliable and precise ambiguity resolution.

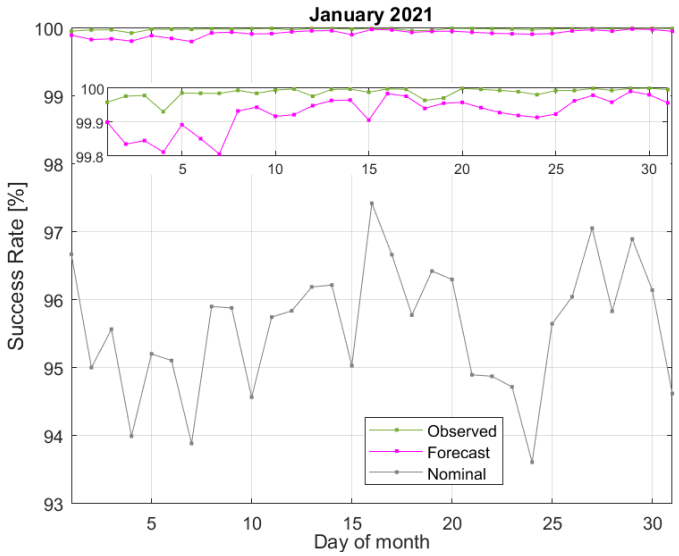

Fig 9. IAR success rates for three scenarios in January 2021 for CUT0 using observed (data-driven) ionospheric process noise, forecasted ionospheric process noise, and the commonly used nominal value (1 $mm/\sqrt{sec}$).

Table 3. Description of GNSS data and parameter configurations for IAR performance evaluation.

GNSS data	
Phase and code data	GPS (L1/L2), Galileo (E1/E5a)
Epoch time	02:00 GPS time (single epoch)
Measurement sampling frequency	1 Hz
Stochastic Model	
Phase zenith-referenced standard deviation	1.0 mm

Code zenith-referenced standard deviation	20 cm
Elevation weighting	Sine function
Elevation cut-off	10°
Dynamic Model	
Phase ambiguities	Time-constant
Satellite biases	Time-constant
satellite clock process-noise	$3\ mm/\sqrt{sec}$
Ambiguity Resolution	
Estimation principle	Integer least squares (ILS)
IAR method	Full IAR with LAMBDA

4. Conclusion

In this study, we utilized an LSTM-based approach to forecast ionospheric process noise and evaluate its effect on IAR performance. Forecasting ionospheric process noise is particularly practical in scenarios where a user station has access to a historical record of ionospheric process noise.

We employed an LSTM neural network to capture the dependencies of ionospheric process noise on solar activity, geomagnetic activity, seasonal variations, and its past behavior (autoregressive). The model demonstrated high performance, with low RMSE values across globally distributed stations, validating its generalizability. The ablation study underscored the importance of combining past target values with external features. However, the significance of specific features varies depending on the geographic location of the station; for example, stations in equatorial regions show higher correlations with solar activity indices, while high-latitude stations are more influenced by geomagnetic activity indices. Our results demonstrate that forecasted ionospheric process noise provides a viable alternative to the nominal value of $1\ mm/\sqrt{sec}$, offering optimal values that effectively enhance IAR performance.

A critical challenge remains in determining the RMSE thresholds that ensure an IAR success rate of 99.9%, a benchmark widely accepted in surveying applications. Future work will address this issue by exploring the relationship between RMSE values and IAR success rates across various stations and conditions.

REFERENCES

Bengio, Y., Simard, P., and Frasconi, P., 1994, Learning long-term dependencies with gradient descent is difficult, IEEE transactions on neural networks, 5(2), pp.157-166, IEEE.

Collins, P., Lahaye, F., and Bisnath, S., 2012, External ionospheric constraints for improved PPP-AR initialisation and a generalised local augmentation concept. In: Proceedings of ION GNSS 2012, Institute of Navigation, Tennessee, USA. 17–21 September, pp 3055–3065.

Goodfellow, I., Bengio, Y., and Courville, A., 2016, Deep Learning, MIT Press.

Hernández-Pajares, M., Juan, J.M., Sanz, J., Aragón-Àngel, À., García-Rigo, A., Salazar, D., and Escudero, M., 2011, The ionosphere: effects, GPS modeling and the benefits for space geodetic techniques, J Geod, 85: 887-907.

Hochreiter, S., and Schmidhuber, J., 1997, Long Short-Term Memory, Neural Computation, 9(8), 1735–1780, Cambridge, MIT Press.

Khodabandeh, A., 2021, Single-station PPP-RTK: correction latency and ambiguity resolution performance, J Geod, 95(4): 42.
Odijk, D., Zhang, B., Khodabandeh, A., Odolinski, R., and Teunissen, P., 2016, On the estimability of parameters in undifferenced, uncombined GNSS network and PPP-RTK user models by means of S-system theory, J Geod, 90(1): 15-44.
Psychas, D., Khodabandeh, A., and Teunissen, P., 2022, Impact and mitigation of neglecting PPP-RTK correctional uncertainty, GPS solute, 26(1): 33.
Ruwali, A., Kumar, A.S., Prakash, K.B., Sivavaraprasad, G. and Ratnam, D.V., 2020, Implementation of hybrid deep learning model (LSTM-CNN) for ionospheric TEC forecasting using GPS data. IEEE Geoscience and Remote Sensing Letters, 18(6), pp.1004-1008.
Sadegh Nojehdeh, P., Khodabandeh, A., Khoshelham, K., and Amiri-Simkooei, A., 2024a, Estimating process noise variance of PPP-RTK corrections: a means for sensing the ionospheric time-variability, GPS Solutions, 28(1), 43, Springer.
Sadegh Nojehdeh, P., Khodabandeh, A., and Khoshelham, K., 2024b, Ionospheric process noise estimation via single-receiver GNSS data, Journal of Spatial Science, 1-20, Taylor & Francis.
Sun, W., Xu, L., Huang, X., Zhang, W., Yuan, T., Chen, Z. and Yan, Y., 2017, July. Forecasting of ionospheric vertical total electron content (TEC) using LSTM networks. In 2017 international conference on machine learning and cybernetics (ICMLC) (Vol. 2, pp. 340-344). IEEE.
Wen, Z., Li, S., Li, L., Wu, B., and Fu, J., 2021, Ionospheric TEC prediction using Long Short-Term Memory deep learning network, Astrophysics and Space Science, 366, pp.1-11.
Wübbena, G., Schmitz, M., and Bagge, A., 2005, PPP-RTK: precise point positioning using state-space representation in RTK networks, In: Proceedings of ION GNSS 2005, Institute of Navigation, Long Beach, CA, USA, pp 2584–2594.
Zha, J., Zhang, B., Liu, T., and Hou, P., 2021, Ionosphere-weighted undifferenced and uncombined PPP-RTK: theoretical models and experimental results, GPS solute, 25(4):135.

BIOGRAPHICAL NOTES

CONTACTS

Parvaneh Sadegh Nojehdeh
University of Melbourne, Parkville, Melbourne, Victoria 3053, Australia
Tel. +61 447 292 239
Email: psadeghnojeh@student.unimelb.edu.au
Web site: https://infrastructure.eng.unimelb.edu.au/people/research-students/geomatics/parvaneh-sadegh-nojehdeh

Kourosh Khoshelham
University of Melbourne, Parkville, Melbourne, Victoria 3053, Australia
Tel. +61 451 038 600
Email: k.khoshelham@unimelb.edu.au
Web site: https://findanexpert.unimelb.edu.au/profile/710868-kourosh-khoshelham